EPJ manuscript No.
(will be inserted by the editor)

Azimuthal Anisotropy of Photon and Charged Particle Emission in ^{208}Pb + ^{208}Pb Collisions at 158 $\cdot A$ GeV/c

WA98 Collaboration

M.M. Aggarwal[4], Z. Ahammed[2], A.L.S. Angelis*[7], V. Antonenko[13], V. Arefiev[6], V. Astakhov[6], V. Avdeitchikov[6], T.C. Awes[16], P.V.K.S. Baba[10], S.K. Badyal[10], S. Bathe[14], B. Batiounia[6], T. Bernier[15], V.S. Bhatia[4], C. Blume[14], D. Bucher[14], H. Büsching[14], L. Carlén[12], S. Chattopadhyay[2], M.P. Decowski[3], H. Delagrange[15], P. Donni[7], M.R. Dutta Majumdar[2], A.K. Dubey[1], K. El Chenawi[12], K. Enosawa[18], S. Fokin[13], V. Frolov[6], M.S. Ganti[2], S. Garpman*[12], O. Gavrishchuk[6], F.J.M. Geurts[19], T.K. Ghosh[8], R. Glasow[14], B. Guskov[6], H. Å.Gustafsson[12], H. H.Gutbrod[5], I. Hrivnacova[17], M. Ippolitov[13], H. Kalechofsky[7], K. Karadjev[13], K. Karpio[20], B. W. Kolb[5], I. Kosarev[6], I. Koutcheryaev[13], A. Kugler[17], P. Kulinich[3], M. Kurata[18], A. Lebedev[13], H. Löhner[8], L. Luquin[15], D.P. Mahapatra[1], V. Manko[13], M. Martin[7], G. Martínez[15], A. Maximov[6], Y. Miake[18], G.C. Mishra[1], B. Mohanty[1], M.-J. Mora[15], D. Morrison[11], T. Moukhanova[13], D. S. Mukhopadhyay[2], H. Naef[7], B. K. Nandi[1], S. K. Nayak[10], T. K. Nayak[2], A. Nianine[13], V. Nikitine[6], S. Nikolaev[13], P. Nilsson[12], S. Nishimura[18], P. Nomokonov[6], J. Nystrand[12], A. Oskarsson[12], I. Otterlund[12], T. Peitzmann[19], D. Peressounko[13], V. Petracek[17], S.C. Phatak[1], W. Pinganaud[15], F. Plasil[16], M.L. Purschke[5], J. Rak[17], R. Raniwala[9], S. Raniwala[9], N.K. Rao[10], F. Retiere[15], K. Reygers[14], G. Roland[3], L. Rosselet[7], I. Roufanov[6], C. Roy[15], J.M. Rubio[7], S.S. Sambyal[10], R. Santo[14], S. Sato[18], H. Schlagheck[14], H.-R. Schmidt[5], Y. Schutz[15], G. Shabratova[6], T.H. Shah[10], I. Sibiriak[13], T. Siemiarczuk[20], D. Silvermyr[12], B.C. Sinha[2], N. Slavine[6], K. Söderström[12], G. Sood[4], S.P. Sørensen[11], P. Stankus[16], G. Stefanek[20], P. Steinberg[3], E. Stenlund[12], M. Sumbera[17], T. Svensson[12], A. Tsvetkov[13], L. Tykarski[20], E.C.v.d. Pijll[19], N.v. Eijndhoven[19], G.J.v. Nieuwenhuizen[3], A. Vinogradov[13], Y.P. Viyogi[2], A. Vodopianov[6], S. Vörös[7], B. Wysłouch[3], and G.R. Young[16]

[1] Institute of Physics, 751-005 Bhubaneswar, India
[2] Variable Energy Cyclotron Centre, Calcutta 700 064, India
[3] MIT Cambridge, MA 02139, USA
[4] University of Panjab, Chandigarh 160014, India
[5] Gesellschaft für Schwerionenforschung (GSI), D-64220 Darmstadt, Germany
[6] Joint Institute for Nuclear Research, RU-141980 Dubna, Russia
[7] University of Geneva, CH-1211 Geneva 4,Switzerland
[8] KVI, University of Groningen, NL-9747 AA Groningen, The Netherlands
[9] University of Rajasthan, Jaipur 302004, Rajasthan, India
[10] University of Jammu, Jammu 180001, India
[11] University of Tennessee, Knoxville, Tennessee 37966, USA
[12] Lund University, SE-221 00 Lund, Sweden
[13] RRC "Kurchatov Institute", RU-123182 Moscow, Russia
[14] University of Münster, D-48149 Münster, Germany
[15] SUBATECH, Ecole des Mines, Nantes, France
[16] Oak Ridge National Laboratory, Oak Ridge, Tennessee 37831-6372, USA
[17] Nuclear Physics Institute, CZ-250 68 Rez, Czech Rep.
[18] University of Tsukuba, Ibaraki 305, Japan
[19] Universiteit Utrecht/NIKHEF, NL-3508 TA Utrecht, The Netherlands
[20] Institute for Nuclear Studies, 00-681 Warsaw, Poland
* Deceased.

the date of receipt and acceptance should be inserted later

Abstract. The azimuthal distributions of photons and charged particles with respect to the event plane are investigated as a function of centrality in ^{208}Pb + ^{208}Pb collisions at 158 $\cdot A$ GeV/c in the WA98 experiment at the CERN SPS. The anisotropy of the azimuthal distributions is characterized using a Fourier analysis. For both the photon and charged particle distributions the first two Fourier coefficients are observed to decrease with increasing centrality. The observed anisotropies of the photon distributions compare well with the expectations from the charged particle measurements for all centralities.

PACS. 25.75.Dw Particle production, azimuthal anisotropy, flow

1 Introduction

Non-isotropic emission of particles with respect to the reaction plane, as first observed at the Bevalac [1], provides evidence for collective flow in high energy heavy ion collisions. Flow, or anisotropic particle emission, has been observed for a large variety of interacting systems from incident energies of a few A GeV/c at the Bevalac (SIS) and AGS to much greater energies at the SPS and RHIC [2,3,4,5,6,7,8,9,10,11,12,13]. The azimuthal anisotropy has been shown to be sensitive to the equation of state of the compressed nuclear matter, although at lower incident energies effects of the momentum dependence of the mean field and the in-medium cross sections have also been shown to be important.

Anisotropic flow manifests itself as asymmetries in the azimuthal distribution of particles and can be reproduced in theoretical models with different underlying assumptions. One scenario is incorporated in transport models where the particles have a mean free path comparable to the system size [14,15]. The models can describe the observed flow up to AGS energies. The other scenario applies when the mean free path is much smaller than the system size which allows the description of the equilibrated system in terms of macroscopic quantities [16,17]. Hydrodynamic models are able to describe the qualitative features of the observed flow [18] for p_T below about 3 GeV/c.

The initial asymmetry in the overlap zone of the colliding nuclei translates into unequal pressure gradients in different directions that leads to an elliptic final state momentum distribution of the particles [16], causing an elliptic pattern of flow. The elliptic flow is therefore expected to be sensitive to the system evolution at the time of maximum compression [19]. The variation of asymmetry with centrality enables to relate the observed flow to the geometry of the overlap region [20,21]. One would then expect a scaling of the data from AGS to SPS and RHIC provided the physics of elliptic flow remains the same [22]. In the case that there is a phase transition from hadronic matter to a quark gluon plasma, it is expected that the reflection of this transition in the equation of state of the dense nuclear matter would result in changes in the pressure gradients which would then be reflected in changes in the particle flow pattern.

The first evidence of azimuthal anisotropy at SPS energies was observed in the distribution of photons from S+Au collisions at 200 $\cdot A$ GeV measured in the preshower photon multiplicity detector of the WA93 experiment at CERN [8]. Since almost 90% of photons produced in ultra-relativistic nuclear collisions originate from the decay of π^0's, the anisotropy of the observed photon distributions should reflect the anisotropy of the π^0 production followed by the effects of decay of the π^0's. Methods have been proposed to estimate the anisotropy of the neutral pion emission by measuring the anisotropy of photons [23]. The decay introduces non-flow correlations between the photon pairs due to four-momentum conservation and may dilute the correlations between the π^0's and the event plane. Determination of the effect of decay enables the deduction of the anisotropy of the neutral pions. The photon anisotropy measurement thus complements the study of the anisotropy of charged particle distributions.

In the present work we report results from the WA98 experiment on the centrality dependence of the anisotropy coefficients extracted from measurement of the azimuthal distributions with respect to the event plane of photons and charged particles in the same pseudorapidity interval. Preliminary results on the anisotropy of photon emission in Pb+Pb collisions have been reported earlier [24,25]. The paper is organized in the following manner: Section 2 describes the experimental setup and data selection. The analysis technique and the results on the centrality dependence of the azimuthal anisotropy of photons and charged particles are discussed in Section 3. Section 4 summarises our investigations.

2 WA98 Experiment and Data Selection

The WA98 experiment at CERN [26] placed emphasis on simultaneous detection of hadrons and photons. The experimental setup consisted of large acceptance hadron and photon spectrometers, detectors for photon and charged particle multiplicity measurements, and calorimeters for transverse and forward energy measurements. The experiment recorded data with 158$\cdot A$ GeV Pb beams from the CERN SPS in 1994, 1995, and 1996. The results presented here are from a portion of the Pb run in 1996 during which the magnet (GOLIATH) was turned off. The analysis presented here used data recorded with the photon multiplicity detector (PMD) and the silicon pad multiplicity detector (SPMD). The data from the mid-rapidity calorimeter (MIRAC) was used to characterize events on the basis of centrality of the collision.

The circular Silicon Pad Multiplicity Detector (SPMD), used for measurement of the charged particle multiplicity, was located 32.8 cm from the target. It had full azimuthal coverage in the region $2.35 \leq \eta \leq 3.75$. The detector had four overlapping quadrants, each fabricated from a single 300 μm thick silicon wafer. The active area of each quadrant was divided into 1012 pads forming 46 azimuthal wedges and 22 radial bins with pad size increasing with radius to provide a uniform pseudo-rapidity coverage. The intrinsic efficiency of the detector was better than 99%. During the datataking, 95% of the pads worked properly. The SPMD was nearly transparent to high energy photons since only about 0.2% are expected to interact in the silicon. Multiple hits of charged particles on a single pad were treated as a single hit for the present analysis. Details of the characteristics of the SPMD can be found in Refs. [27,28].

The photon multiplicity was measured using the preshower photon multiplicity detector (PMD) located at a distance of 21.5 meters from the target. The detector consisted of 3 radiation length (X_0) thick lead converter plates placed in front of an array of square scintillator pads of four different sizes that varied from 15 mm$\times$15 mm to 25 mm$\times$25 mm, placed in 28 box modules. Each box module had a matrix of 38×50 pads which were read out using one image intensifier + CCD camera. Details of the design and characteristics of the PMD may be found in Ref. [29,30].

The clusters of hit pads with a signal above a hadron rejection threshold were identified as photon-like. The present analysis has been performed with the photon-like clusters, which are referred to as photons for brevity. Detailed simulations showed that the photon counting efficiencies for the central to peripheral cases varied from 68% to 73%. The purity of the photon sample in the two cases varied from 65% to 54%. Most of the contaminants of the photon sample are charged particles which

Table 1. Centrality selections used in the present analysis based on the measured total transverse energy. The corresponding fraction of the minimum bias cross section, number of participants, and the average photon and charged particle multiplicities measured in the pseudorapidity interval $3.25 \leq \eta \leq 3.75$ are given for each centrality selection.

E_T(GeV)	% σ_{MB}	N$_{part}$	$< N_{photon} >$	$< N_{hits} >$
40.0- 89.9	50-80	43.7	41.1	34.3
89.9-124.3	40-50	87.5	65.6	56.9
124.3-170.2	30-40	123.0	88.0	78.1
170.2-225.5	20-30	172.2	116.9	105.5
225.5-298.6	10-20	237.7	163.1	150.5
298.6-347.6	5-10	300.4	190.1	177.1
>347.6	0-5	353.4	222.9	210.3

deposit enough energy to fall above the hadron rejection threshold. The hadron rejection threshold is taken as three times the energy deposited by a minimum ionizing particle. For photons this leads to a low p$_T$ threshold of 30 MeV/c.

The transverse energy was measured with the MIRAC calorimeter [31] located at 24.7 meters downstream from the target. The MIRAC was used to measure the total transverse energy by measurement of both the transverse electromagnetic ($E_{\rm T}^{em}$) and hadronic ($E_{\rm T}^{had}$) energies in the pseudorapidity interval $3.5 \leq \eta \leq 5.5$. The measured total transverse energy, $E_{\rm T}$, provides a measure of the centrality of the reaction. Events with large $E_{\rm T}$ correspond to very central reactions with small impact parameter, and vice versa.

The minimum bias $E_{\rm T}$ distribution has been divided into different fractions of the minimum bias cross section corresponding to different centrality bins [30]. The most central selection corresponds to that 5% of the minimum bias cross section $\sigma_{\rm MB}$ with largest measured $E_{\rm T}$. A total of about 0.25 Million events have been analysed. The minimum number of events in any centrality selection is 15K and the maximum is 70K. Table 1 shows the percentage cross section and the corresponding number of participants for each centrality bin. The results presented here use only the data for the pseudorapidity region of common coverage of the PMD and SPMD ($3.25 \leq \eta \leq 3.75$) where both detectors have full azimuthal coverage. The average measured photon and charged particle multiplicities for this region of acceptance are also quoted for each centrality in Table 1.

3 Analysis

The anisotropy of the azimuthal distribution of particle emission with respect to the reaction plane (or event plane) is characterized by the coefficients of the Fourier expansion of the azimuthal distribution [32]. The first and the second coefficients are measures of the directed and elliptic flow when the expansion is made about the reaction plane, the plane defined by the beam direction and the impact parameter. This may be written as

$$\frac{2\pi\, dN}{d(\phi - \psi_R)} = 1 + 2v_1 \cos(\phi - \psi_R) + 2v_2 \cos 2(\phi - \psi_R) \quad (1)$$

where ϕ is the azimuthal angle of the measured particle and ψ_R denotes the azimuthal orientation of the reaction plane. The reaction plane is best determined in an experiment that measures the (transverse) momenta of the target or projectile fragments. Both v_1 and v_2 can take positive or negative values. By convention, positive (negative) values of v_1 in equation 1 denote flow (anti-flow) in the direction of the deflected projectile fragment, and positive (negative) values of v_2 indicate in-plane (out-of-plane) flow.

Though the best determination of the reaction plane requires the measurement of target (or projectile) fragments, most experiments *assume* that the measurement of any particle type, in any kinematic window enables a determination of the reaction plane. We wish to distinguish between the plane determined by projectile or target fragments and the plane determined by any other particle type, and throughout this article refer to the latter as the *event plane*. Obtaining the values of coefficients after projecting azimuthal angles on the event plane determined from the same set (after removing auto correlations) maximises the values of anisotropy coefficients, and may include non-flow correlations. The values obtained are necessarily positive, and have been shown as such in the present work. The coefficients determined by projecting on an event plane from any other set of particles are expected to be smaller, and can also have negative values. The difference in the values determined using different sets of event planes have been included in systematic error by various experiments [10,11,13].

3.1 Method

In the present analysis, the shape of the azimuthal distributions of particle emission for any particle species in any pseudorapidity window is characterized by an ellipse. The direction of the centroid and the major axis of the ellipse are determined from the azimuthal distributions of the particles. These directions, along with the beam direction, define the first order and the second order event plane respectively, and are obtained as [32]

$$\psi'_m = \frac{1}{m}\left(\tan^{-1}\frac{\Sigma w_i \sin m\phi_i}{\Sigma w_i \cos m\phi_i}\right) \quad (2)$$

where m = 1 or 2 for the first and the second order, respectively. The ϕ_i are the azimuthal angles of the emitted particles with respect to a fixed laboratory direction and the w_i are the weight factors. For the azimuthal distribution of the particle yield, as in equation 1, the weight factors are set equal to one. In reality, due to finite particle multiplicities ψ'_1 and ψ'_2 fluctuate about the *actual* event planes that represent the direction of the centroid and the direction of the major axis of the elliptic shape. To the extent that initial state nuclear densities are spherically symmetric and the density fluctuations are negligible, the initial nucleon density in the overlap region is symmetric about the impact parameter or reaction plane and so it is expected that the two event plane angles are either the same or perpendicular to the reaction plane.

The anisotropy, or Fourier coefficients of order n, can be determined from the azimuthal distribution of the particles with

respect to the event plane angle of order m, provided n is an integral multiple of m, by fitting to the following equations [32]

$$\frac{dN}{d(\phi-\psi'_m)} \propto 1+\sum_{n=1}^{\infty} 2v'_{nm}\cos nm(\phi-\psi'_m) \qquad (3)$$

v'_{nm} is a measure of the offset of the centroid of the distribution when $n \cdot m$ = 1 and is a measure of the difference between the major and the minor axes of the ellipse when $n \cdot m$ = 2. The actual coefficients are obtained from the observed coefficients v'_{nm} as described later.

Since the event planes do not depend on the geometrical setup of the experiment, the distribution of the event plane angles determined for a large number of events is expected to be uniformly distributed in laboratory angle. Any non-uniformity in the acceptance of the detectors over the full azimuth will be reflected in a non-uniform distribution of event plane angles. Any such non-uniformity that remains constant during the data taking period can be corrected for by appropriate correction methods. The method employed in the present work is summarized in the following.

3.2 Detector Acceptance Correction

The corrected event plane angle is obtained by shifting the observed event plane angles ψ'_m by $\Delta\psi'_m$ [32] where the latter is written as

$$\Delta\psi'_m = \sum_{n=1}^{N}\frac{2}{nm}(-\langle\sin(nm\,\psi'_m)\rangle\cos(nm\,\psi'_m) + \langle\cos(nm\,\psi'_m)\rangle\sin(nm\,\psi'_m)) \qquad (4)$$

where $N = 4/m$ is sufficient to flatten the raw ψ distribution. The angular brackets denote an average over all events and are obtained from the raw distribution of the m^{th} order event plane distribution.

The distribution of the first and the second order event plane angles, corrected for acceptance, is shown in Fig. 1 for photon hits in the PMD and in Fig. 2 for hits in the SPMD.

3.3 Event Plane Resolution Correction

The average deviation of the estimated event plane from the true event plane due to multiplicity fluctuations can be determined experimentally and is termed as the resolution correction factor (RCF). Experimentally, RCF is obtained using the subevent method described in [32]. Here every event is divided randomly into two subevents of equal multiplicity and the event plane angle ψ'_m is determined for each subevent.[1]

This enables determination of a parameter χ_m directly from the experimental data using the fraction of events where the correlation of the planes of the subevents is greater than $\pi/2$ [32,33]:

$$\frac{N_{events}(m|\psi'^a_m-\psi'^b_m|>\pi/2)}{N_{total}} = \frac{e^{-\frac{\chi_m^2}{4}}}{2} \qquad (5)$$

where N_{total} denotes the total number of events, ψ'^a_m, ψ'^b_m are the observed event plane angles of the two subevents (labeled a and b) and the numerator on the left denotes the number of events having the angle between subevents greater than $\pi/2m$. The parameter χ_m so obtained is then used to determine RCF$_{nm}$ = $\langle\cos(nm(\psi'_m-\psi^{true}_m))\rangle$, where ψ^{true}_m is the true direction of the event plane, and the average is over all events. The RCF can be determined from χ_m by the following relation from reference [32].

$$\langle\cos(nm(\psi'_m-\psi^{true}_m))\rangle = \frac{\sqrt{\pi}}{2\sqrt{2}}\chi_m\exp(-\chi_m^2/4)\cdot\left[I_{\frac{n-1}{2}}(\chi_m^2/4)+I_{\frac{n+1}{2}}(\chi_m^2/4)\right] \qquad (6)$$

where I_ν are the modified Bessel functions of order ν. For the data sample used in the present analysis, the minimum and the maximum values of the resolution correction factors for the photon distributions are 0.36 and 0.41 for the first order and 0.37 and 0.43 for the second order. The corresponding values for SPMD hits are 0.10 and 0.27 for first order and 0.16 and 0.33 for the second order. The errors on the RCF values have been obtained by considering that the error on N_{events} is statistical. The new values of χ_m are then calculated for values of $N_{events} \pm \sqrt{N_{events}}$ and used in equation 6 to calculate new values of RCF. The change in the RCF values gives the statistical error on the RCF determination. In general, the errors determined in this way are asymmetric. Symmetric errors have been quoted using the larger of the two asymmetric errors.

3.4 Anisotropy Coefficients

The anisotropy coefficients are obtained from the particle azimuthal distributions with respect to the event planes determined using the same set of particles. Auto correlations are avoided by extracting the event plane from all particles excluding the particle being entered into the distribution.

The anisotropy coefficients have been determined by three methods which differ in detail and provide a consistency check. In this analysis the Fourier coefficients prior to event plane resolution correction v'_{nm} are extracted for the case with event plane order equal to the order of the extracted Fourier coefficient, i.e. v'_{nm} = v'_{nn} which we will denote by v'_n. In the first method we determine

1. v'_1 = $\langle\cos(\phi-\psi'_1)\rangle$: a measure of the shift in centroid in the direction of ψ_1,
2. v'_2 = $\langle\cos 2(\phi-\psi'_2)\rangle$: a measure of the ellipticity about ψ_2,

where the average is over all particles of all events. This determines the magnitude of the coefficients and is necessarily positive.

[1] The distribution of the corrected event plane angles for these subevents is observed to be flat, for both orders, for photons and for charged particles.

The distributions with respect to the first order event plane are shown in Fig. 3 for both photon and charged particles, for all centralities. In the second method the distributions have been fitted to equation 3 to determine v'_{11}. The corresponding distributions with respect to the second order event plane are shown in Fig. 4 and have been fitted to equation 3 to determine v'_{22}. For both orders, the fits have been made keeping terms up to values of n · m = 2 in the summation in equation 3.

The v'_n values obtained by computing the averages over the distributions are in good agreement with the values obtained from fits to the distributions of Fig.3 and Fig.4.

The v'_{nm} are the values determined with respect to the estimated event plane and must be corrected for the event plane resolution [32] to obtain the actual anisotropy values

$$v_{nm} = \frac{v'_{nm}}{RCF_{nm}} \tag{7}$$

In the third method, the event-plane resolution corrected values v_{nn} have been obtained directly by the subevent method from χ_m of Eq. 5 and the fluctuation in the average multiplicity M of the full events in that centrality bin.

$$v_{nn} = \frac{\chi_n}{\sqrt{2M}} \tag{8}$$

The v_n (= v_{nn}) values obtained by the different methods are compared in Fig. 5 for the different centralities. The different methods yield consistent results for both the first order and the second order anisotropy coefficients. In the following, only the results obtained by the Fourier fit of the azimuthal distributions with respect to the event planes are presented. The following sections discuss the systematic effects that distort the measured anisotropies and the centrality dependence of the anisotropies for charged particles and for photons.

4 Anisotropy in Charged Particles

The measured anisotropy is expected to be less than the actual anisotropy due to the finite granularity of the detector. The measured values of anisotropy may also be affected by the imprecision in the vertex position due to the finite spread of the beam. These effects are particularly relevant for the charged particle distribution measurement due to the relatively coarse segmentation and close proximity to the target of the SPMD detector. The effects are estimated using simulations.

4.1 Granularity

The finite granularity of the SPMD detector causes a dilution of the anisotropy of the azimuthal distribution primarily due to efficiency losses from multiple hits and also due to the associated decreased angular resolution. The quantitative effect of the finite granularity on the measured anisotropy has been estimated by simulations, by methods described in greater detail in [34]. The azimuthal distributions of the charged particles were generated with different initial anisotropies with multiplicities corresponding to the measured results. The charged particle hits were sorted into the SPMD bins (2° ϕ-bin) assuming a 94% detection efficiency but taking into account hit losses due to multiple hits in a single SPMD pad. The resulting azimuthal distributions were then analyzed to determine the anisotropy coefficients using the method detailed in Sec 3.4 above. Fig. 6 shows the results of the simulation for both orders, where the anisotropy coefficients extracted from the hit distribution is shown for varying initial anisotropy. The solid lines are polynomial fits to the simulated data. The simulation results show that the extracted anisotropy is systematically lower than the initial anisotropy. Part of this loss occurs directly due to efficiency losses from multiple hits, and contributes both to the anisotropy and the event plane resolution. In addition to the different quantitative contribution of the multiple hits to the event plane resolution and the anisotropy values, there is another contribution that arises from the process of removing auto correlations. Here the event plane is estimated for every particle by removing the particle in question. For the present case this is equivalent to removing a pad, which in effect removes all other particles falling within that pad due to multiple hit probability, while retaining all other hit pads. The resultant effect is to add a negative correlation thereby underestimating the values of the extracted anisotropies. These simulation results enable a determination of the actual anisotropy from the measured anisotropy for this experiment and the results are discussed in the following sections.

4.2 Shift in Vertex and Beam Spread

The finite beam size caused an imprecision in the assumed vertex by up to one mm in the WA98 experiment. A small shift in the vertex position does not affect the azimuthal distribution in the fine granularity PMD, situated at 21.5 meters from the vertex. However, it can produce an apparent anisotropy in the hit distribution in the SPMD situated at 0.328 meters from the target.

The effect of vertex shifts due to the beam spread was also investigated by simulation. The vertex position was generated according to a two dimensional Gaussian with width σ. Particles were simulated to originate from this vertex position with a realistic η and p_T distribution and an azimuthally symmetric ϕ distribution. The particles were projected onto the SPMD plane, and their hit positions recorded according to the granularity and nominal location of the SPMD detector. The recorded positions corresponded to values of η and ϕ which differed from the generated values due to the shifted position of the vertex. The simulated distributions were then analyzed in the same manner as the experimental data. This was repeated for different values of σ and the values of v_n were obtained for each sample generated. The maximum possible shift could be deduced by using the result that the measured value of v_1 for the most central class is consistent with zero. This corresponded to a maximum width of the Gaussian distribution due to beam spread of 0.4 mm.

A shift in the vertex position due to beam spread, or time variation during the 2.5 s SPS spill, produces an azimuthal distribution which has a shifted centroid. If the shift occurs on

an event-by-event basis it cannot be corrected for by the acceptance correction methods discussed above, since they can only correct for average effects. To investigate the possibility of systematic shifts correlated with time during the SPS spill, the SPMD charged particle azimuthal distributions were analyzed for different times during the spill. No significant variations with time during the spill were observed.

The second order anisotropy is obtained from the fit to the elliptical shape of the measured hit distribution. A vertex shift does not affect the elliptical shape, as verified by simulations.

4.3 Results

The finite granularity requires a correction which is obtained using the measured values of v_n from the hit distributions and the calibration figure obtained using simulations and shown in Fig. 6. The corrected results are shown for both orders of anisotropy in Fig. 7. The systematic error due to the granularity correction is obtained by changing the order of the polynomial to the fit in Fig. 6, and lies within the size of the symbol. The error bars shown are statistical. The results for the first order anisotropy include contributions from a possible vertex shift. The upper and the lower limit of the boxes shown in Fig 7a show the asymmetric systematic error and correspond to no uncertainty and a maximum uncertainty in the position of the vertex, as discussed above.

For the most central event selection (top 5% of the minimum bias cross section) the measured charged particle anisotropy was observed to be consistent with zero for both orders (see Figs. 3 and 4). The simulation results show that the actual anisotropy in this case is less than 2.6% for the first order and less than 2.3% for the second order, which is the limit of sensitivity of the SPMD detector for the experimental conditions discussed here. The shaded region for the most central bin marks the upper limit of the possible anisotropy consistent with the measured value of zero for both orders.

Fig. 8 shows v_2 as a function of centre of mass energy. These have been measured in different experiments in different kinematic ranges using methods that vary in detail. The broad behaviour shows a continuous increase in v_2 as a function of centre of mass energy. The results of the present work are shown for two different centrality ranges corresponding to 10-20% of cross section and 10-30% of cross section. For comparison to the present results, values of v_2 for NA49 and CERES at the same centre of mass energy are included. The present results are slightly higher than those from other exprimments. These differences are not unexpected considering the variations in the centrality selections, kinematic selections and the different quantitative contribution from other sources to the measured values of v_2. e.g.results of NA49 experiment quote v_2 for pions determined using p_T as weight factors. This decreases the bias due to Bose-Einstein correlations [37] The NA49 results have a 15% systematic error in addition. The present work uses number distribution of charged particles and the results shown include systematic errors.

5 Anisotropy in Photons

The photons incident on the PMD predominantly result from the two photon decay of the neutral pion, and if both photons are detected in the PMD an additional apparent anisotropy will result from the kinematic correlation between the photons. The limited efficiency and purity of the detected photon sample in the PMD affect the measured photon anisotropy values. The quantitative effect is estimated using simulations and is described in the following.

5.1 Decay Effect

The decay of neutral pions into two photons introduces correlations that can cause apparent anisotropies in the photon distributions which are greater than the actual anisotropy of the pions. On the other hand, the process of decay smears the photon momenta relative to the initial pion momenta and can thereby dilute the initial correlation present in the neutral pions. The relative importance of these two competing effects has been shown to scale with the experimentally measured quantity χ_m and enables a determination of the neutral pion anisotropy from the measured photon anisotropy [23]. The relationship between the γ and π^0 anisotropy is sensitive to the acceptance of the detector, particularly if the multiplicity and the anisotropy are small. The ratio of the γ anisotropy corresponding to a given π^0 anisotropy is a steep function of χ_m in the region where the values of χ_m are less than about 1.0 for v_1 and about 0.6 for v_2. The results in the present work correspond to this region of χ_m, resulting in large uncertainties in the relationship between the π^0 anisotropy and the measured γ anisotropy. However, it is possible to compare the anisotropy values of photons to the values obtained from charged particles, as discussed below.

5.2 Efficiency and Contamination

The PMD records particle hits which include incident photons and a contamination of charged particle hits. These charged particles could be primary, or secondary rescattered particles. As noted above, the photon counting efficiency (e) of the sample varies from 68% to 73% for central and peripheral events and the corresponding purity (p) of the sample varies from 65% to 54%.

The effect of decay, identification efficiency, and contamination on the observed photon anisotropy has been estimated using simulations. The simulations assume that the photon sample contains a contribution from charged particle contamination which directly reflects the measured charged particle anisotropy in addition to a contribution from photons from π^0 decays with a π^0 anisotropy which is also equal to the measured charged particle anisotropy. These simulations use the anisotropy values of the charged particles, π^0 decay kinematics, the PMD acceptance, and the purity of the PMD photon sample to generate simulated data. The simulated sample is analyzed to obtain an estimate of the expected photon anisotropy corresponding to the observed charged particle anisotropy.

The neutral pions were generated using the experimental pseudorapidity distribution of the charged pions [35] with an

exponential p_T distribution (dN/dp_T = $p_T \cdot$ exp(-6p_T)). The π^0 multiplicity and anisotropy values were chosen as those measured for the charged particles with the SPMD for the same centrality selection. Neutral pions were generated and decayed and the decay photons were accepted if within the PMD acceptance. Using the measured photon multiplicity for a given centrality class, $p \cdot N_{photons}$ photons were randomly selected from those falling onto the PMD, where p was assigned a value of 0.65 to 0.54 corresponding to the centrality selection being simulated. A background contribution of $(1-p) \cdot N_{photons}$ charged particles was added to the simulated event. This simulated data was then analyzed using the methods detailed in section 3.4.

The systematic errors in the simulated results have been estimated for both orders of anisotropy for each centrality. The percentage systematic error is largest for the most central events because the measured values of charged particle anisotropy are consistent with zero. For all other classes the maximum systematic error due to various sources for both orders is shown in Table 2. The contribution to the systematic error for one particular centrality selection (10%-20% of minimum bias cross section) is shown in Table 3.

The systematic error on the measured values of v_n^{PMD} have been obtained by

- increasing and decreasing the region of acceptance for the analysis
- calculating the resolution correction factor by random division into subevents and by dividing into subevents according to η values
- randomly removing up to 40% of the photons in the PMD

The analysis was repeated by rejecting clusters closer than twice the size of the scintillator pads and the resulting change is included in the systematic errors shown in the figure.

Table 2. Largest value of systematic error for each systematic error for both orders of anisotropy of the $N_{photons}$ distributions for *any* centrality selection.

Source	First Order	Second order
	+13.3%	+16.9%
Charged Particle Anisotropy		
	-42.6%	-11.6%
Purity of photon Sample	±15.9%	±14.0%
p_T Dependence of Initial Anisotropy	-	±10.2%
Anisotropy of Contaminants	-20.0%	-27.5%
η and p_T distribution of π^o	±3%	±2.8%
Neutral Pion Multiplicity	±14.2%%	±25.7%

5.3 Results

The measured values of v_n^{PMD} are shown in Fig. 9. The open triangles show the expected values of v_n^{PMD} from the simulations described above. These include the effect of decay correlations. The present method includes certain non-flow correlations which affect the two orders of anisotropy differently. The simulations include most of these effects. The statistical and systematic errors are added in quadrature. The errors on the simulated data are shown by the shaded regions. The v_1 and v_2 anisotropy coefficients extracted from the simulated PMD data are consistent within errors with the measured PMD result.

Table 3. Contribution to systematic error from various sources for both orders of anisotropy of the $N_{photons}$ distributions for the centrality selection corresponding to 10-20% of minimum bias cross section.

Source	First Order	Second order
	+2.7%	+10.7%
Charged Particle Anisotropy		
	-19.8%	-7.9%
Purity of photon Sample	±5.7%	±7.2%
p_T Dependence of Initial Anisotropy	-	±8.8%
Anisotropy of Contaminants	-20%	-22%
η and p_T distribution of π^o	±3%	±2.8%
Neutral Pion Multiplicity	±1.6%	±6.1%

Measured values of v_2^{PMD} are shown in Fig. 10 as a function of N_{part}. The flow coefficient measured in the electromagnetic calorimeter LEDA [36], covering the photon rapidity region $2.3 \leq y \leq 2.9$. are also shown for comparison. One must mention here that the v_2 coefficients obtained in LEDA are by projecting the angles of the photons on the reaction plane obtained using the target fragments and the values measured in the PMD are obtained as described in section 3 in this manuscript. The difference in the two results for the most central sample may be due to the difference in the analysis techniques used in the two cases where the reaction planes have been obtained differently.

6 Summary

The azimuthal angle distributions with respect to the event plane have been measured for charged particles and photons with full azimuthal coverage in the pseudorapidity region of 3.25 $\leq \eta \leq$ 3.75 for ^{208}Pb + ^{208}Pb collisions at 158 $\cdot A$ GeV/c. A total of 0.25 million events, classified in seven centrality selections, have been used in the analysis. The Fourier coefficients of the azimuthal distributions have been extracted in several ways, all giving consistent results for the first order v_1 (directed) and v_2 second order (elliptic) anisotropies for photons and charged particles. The results show the expected trend of decreasing anisotropy with increasing centrality for both v_1 and v_2 for charged particles and photons. Our results for charged particle anisotropy are slightly higher than the correspondineg values for pions reported by NA49 collaboration [37]. This difference may arise due to (a) inclusion of protons in the charged particle sample in the present work, where the anisotropy in protons also depends upon both p_T and the centrality selection [38],(b) HBT and other non-flow effects which are known to contribute to the measured values of anisotropy

and (c) the NA49 results are based on using transverse momentum as the weight in the determination of the coefficient, whereas the present work measures the azimuthal distribution of the number of particles and assumes all weight factors to be equal. The present results are lower than the values obtained for charged particles at RHIC energies by the PHOBOS collaboration [13]. The observed anisotropies of the photon distributions are comparable to the charged particle anisotropies. The photon distributions contain contributions mainly from π^0 decay and charged particle contamination. The observed anisotropies of the photon distributions compare well with those obtained from simulations that include the charged particle contamination and the decay of neutral pions assumed to have the same anisotropies as measured for charged particles.

We wish to express our gratitude to the CERN accelerator division for the excellent performance of the SPS accelerator complex. We acknowledge with appreciation the effort of all engineers, technicians, and support staff who have participated in the construction of this experiment.

This work was supported jointly by the German BMBF and DFG, the U.S. DOE, the Swedish NFR and FRN, the Dutch Stichting FOM, the Polish KBN under Contract No. 621/E-78/SPUB-M/CERN/P-03/DZ211/, the Grant Agency of the Czech Republic under contract No. 202/95/0217, the Department of Atomic Energy, the Department of Science and Technology, the Council of Scientific and Industrial Research and the University Grants Commission of the Government of India, the Indo-FRG Exchange Program, the PPE division of CERN, the Swiss National Fund, the INTAS under Contract INTAS-97-0158, ORISE, Grant-in-Aid for Scientific Research (Specially Promoted Research & International Scientific Research) of the Ministry of Education, Science and Culture, the University of Tsukuba Special Research Projects, and the JSPS Research Fellowships for Young Scientists. ORNL is managed by UT-Battelle, LLC, for the U.S. Department of Energy under contract DE-AC05-00OR22725. The MIT group has been supported by the US Dept. of Energy under the cooperative agreement DE-FC02-94ER40818.

References

1. H. A. Gustafsson et al., Phys. Rev. Lett. **52** (1984) 1590; H. H. Gutbrod et al., Phys. Lett. **B216** (1989) 267; H. H. Gutbrod et al., Rep. Prog. Phys. **52** (1989) 1267; H. H. Gutbrod et al., Phys. Rev. **C42** (1990) 640.
2. W. Reisdorf and H.G. Ritter, Ann. Rev. Nucl. Part. Sci **47** (1997) 663.
3. EOS Collaboration, J.Chance et al., Phys. Rev. Lett. **78** (1997) 2535; M.A.Lisa et. al., nucl-ex/**9610007**.
4. FOPI Collaboration, G. Poggi et al., Nucl. Phys. **A586** (1995) 755, J. L. Ritman et al., Z. Phyc. **352** (1995) 355; N. Bastid et al., Nucl. Phys. **A622** (1997) 573.
5. KaoS Collaboration, D. Bril et al., Phys. Rev. Lett. **71** (1993) 336; D. Brill et al., Z. Phys. **A355** (1996) 61; Y. Shin et al., Phys. Rev. Lett. **81** (1998) 1576.
6. E877 Collaboration, J.Barette et.al., Phys. Rev. Lett. **73** (1994) 2532; Phys. Rev. Lett. **70** (1993) 2996; Phys. Rev. **C55** (1997) 1420; Phys. Rev. **C56** (1997) 3254.
7. E802 Collaboration, L.Ahle et.al., Phys. Rev. **C57** (1998) 1416.
8. WA93 Collaboration, M.M.Aggarwal et.al., Phys. Lett. **B403** (1997) 390.
9. WA98 Collaboration, M.M.Aggarwal et.al., Phys. Lett. **B469** (1999) 30.
10. NA49 Collaboration, T. Wienold et al., Nucl. Phys. **A610** (1996) 76c; H. Appelshäuser et al., Phys. Rev. Lett. **80** (1998) 4136.
11. STAR Collaboration, K.H. Ackermann et al., Phys. Rev. Lett **86** (2001) 402; C. Adler et al., Phys. Rev. Lett.**87** (2001) 182301.
12. PHENIX Collaboration, K. Adcox et al., Phys. Rev. Lett.**89** (2002) 212301. S. Esumi et al., Nucl. Phys. **A715** (2003) 599c.
13. PHOBOS Collaboration, B.B. Back et.al., Phys. Rev. Lett. **89** (2002) 222301.
14. P. Danielewicz et.al., Phys. Rev. Lett. **81** (1998) 2438; Nucl. Phys. **A661** (1999) 82c.
15. G.Q. Li, C.M. Ko and B. Li, Phys. Rev. Lett. **74** (1995) 235; H.Sorge, Phys. Rev. **C52** (1995) 3291.
16. J.-Y. Ollitrault, Phys. Rev. **D46** (1992) 229.
17. P.F. Kolb et.al., Nucl. Phys. **A696** (2001) 197.
18. P.F. Kolb, J. Sollfrank and U.W. Heinz, Phys. Rev. **C62** (2000) 054909.
19. H. Sorge, Phys. Rev. Lett. **78** (1997) 2309.
20. H. Sorge, Phys. Rev. Lett. **82** (1999) 2048.
21. H. Heiselberg and Anne-Marie Levy, Phys. Rev. **C59** (1999) 2716.
22. S.A. Voloshin and A.M. Poskanzer, Phys. Lett. **B474** (2000) 27.
23. R. Raniwala, S. Raniwala, and Y.P. Viyogi, Phys. Lett. **B489** (2000) 9.
24. Gobinda Mishra, Ph.D thesis, Utkal University, 1999.
25. Sudhir Raniwala, Pramana-Journal of Physics **60** (2003) 739.
26. *Proposal for a Large Acceptance Hadron and Photon Spectrometer*, Preprint CERN/SPSLC 91-17, SPSLC/P260.
27. WA98 Collaboration, M.M. Aggarwal et al., Phys. Lett. **B420** (1998) 169.
28. W.T. Lin et al., Nucl. Instrum. Meth. **A389** (1997) 415.
29. M.M. Aggarwal et al., Nucl. Instrum. Methods Phys. Res. **A424** (1999) 395.
30. WA98 Collaboration, M.M. Aggarwal et al., Phys. Lett. **B458** (1999) 422.
31. T. C. Awes et al., Nucl. Instrum. Methods Phys. Res. Sect. A **279** (1989) 497.
32. A.M. Poskanzer and S. Voloshin, Phys. Rev. **C58** (1998) 1671.
33. J.-Y. Ollitrault, e-print nucl-ex/**9711003**.
34. R. Raniwala, S. Raniwala, and Y.P. Viyogi **ALICE-INT-2001-49** (2001).
35. WA98 Collaboration, M.M. Aggarwal et al., Eur. Phys. J. **C18** (2001) 651.
36. WA98 Collaboration, S.Nikolaev et al., Nucl.Phys. **A715** (2003) 579c; WA98 Collaboration, under preparation
37. NA49 Collaboration, C. Alt et al., Phys.Rev.**C68** (2003) 034903.
38. CERES/NA45 Collaboration, J. Slivova et al., Nucl. Phys. **A715** (2003) 615c.

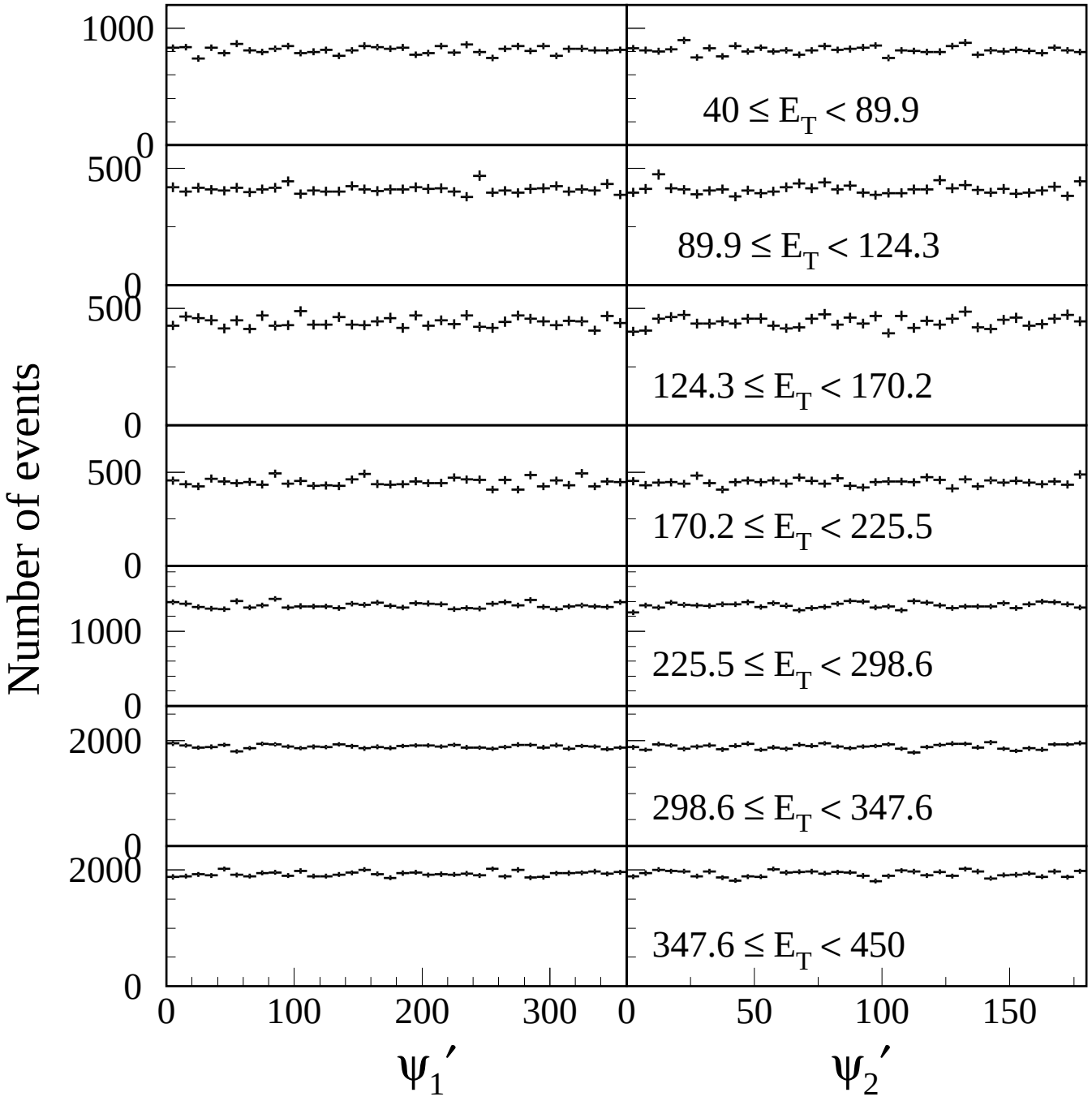

Fig. 1. Acceptance corrected distributions of (a) the first order event plane angle, ψ_1', or (b) the second order event plane angle, ψ_2', determined from photons in the PMD in the region $3.25 \leq \eta \leq 3.75$ for various centralities

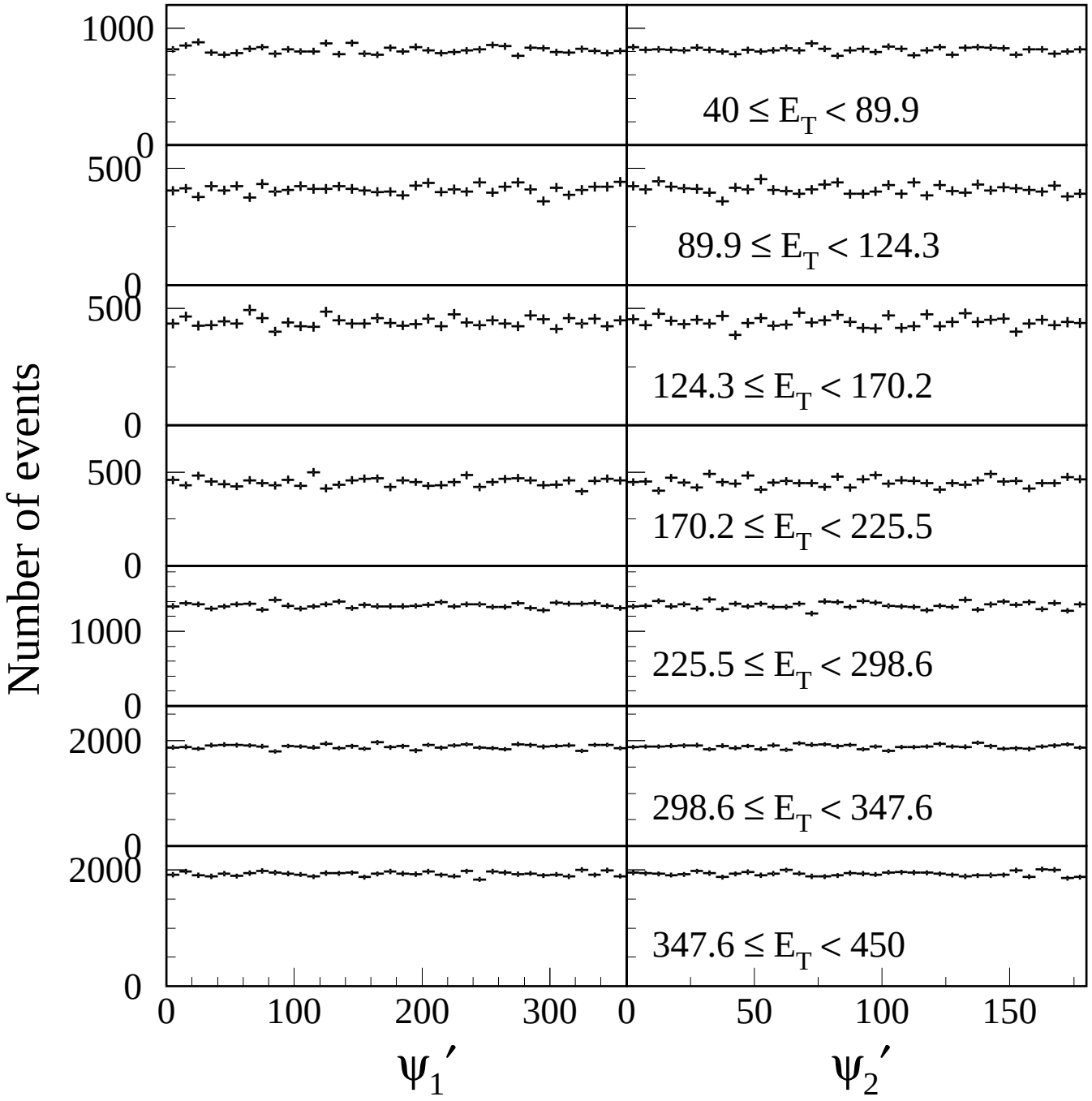

Fig. 2. Acceptance corrected distributions of (a) the first order event plane angle, ψ_1', or (b) the second order event plane angle, ψ_2', for various centralities determined from charged particle hits in the SPMD in the region $3.25 \leq \eta \leq 3.75$.

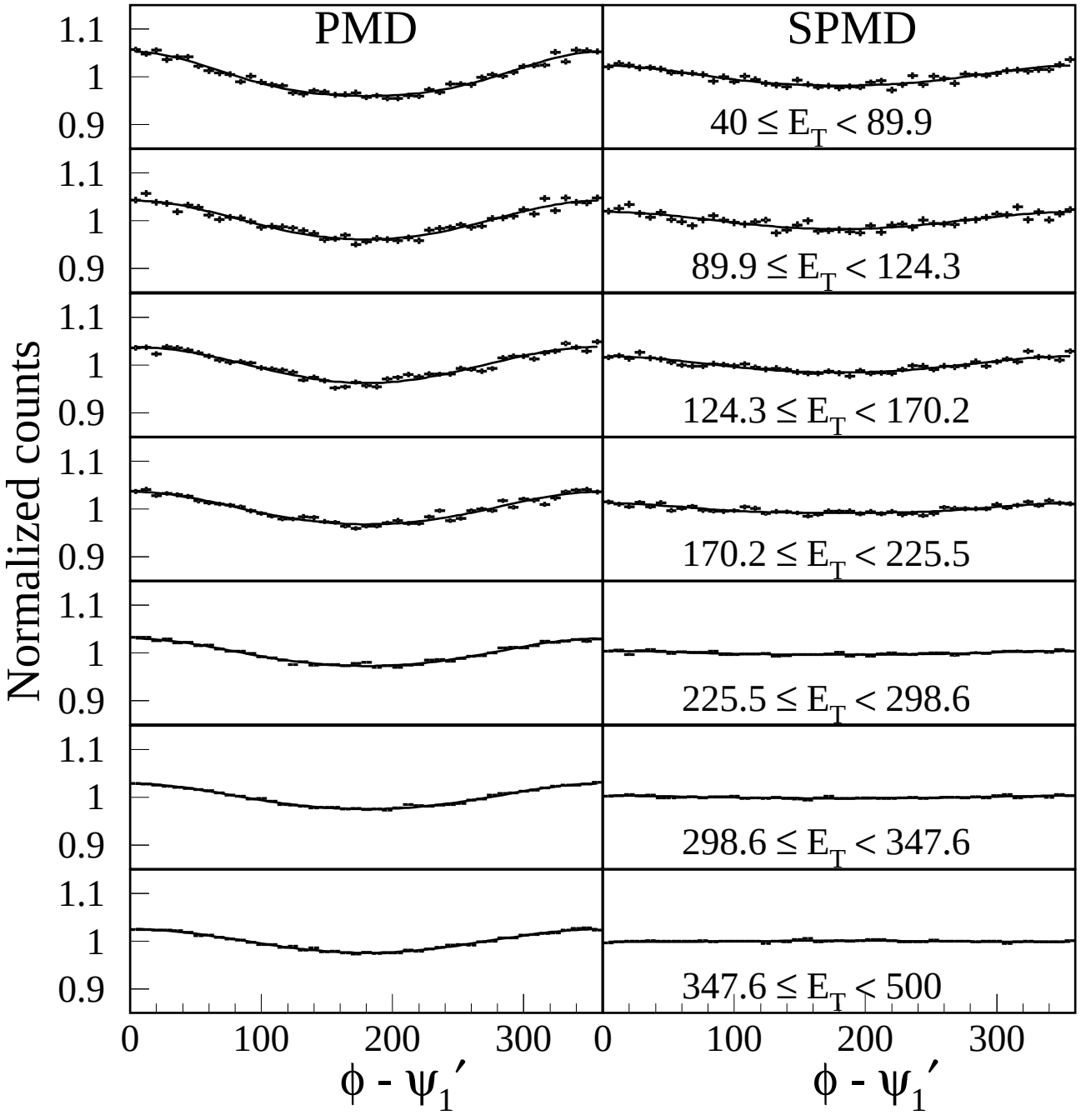

Fig. 3. Distributions of azimuthal angles with respect to the first order event plane, ψ_1', (a) for photons in the PMD and (b) for charged particle hits in the SPMD. Results are shown for each centrality selection in the pseudorapidity region $3.25 \leq \eta \leq 3.75$. The fit results using Eq. 3 are also shown.

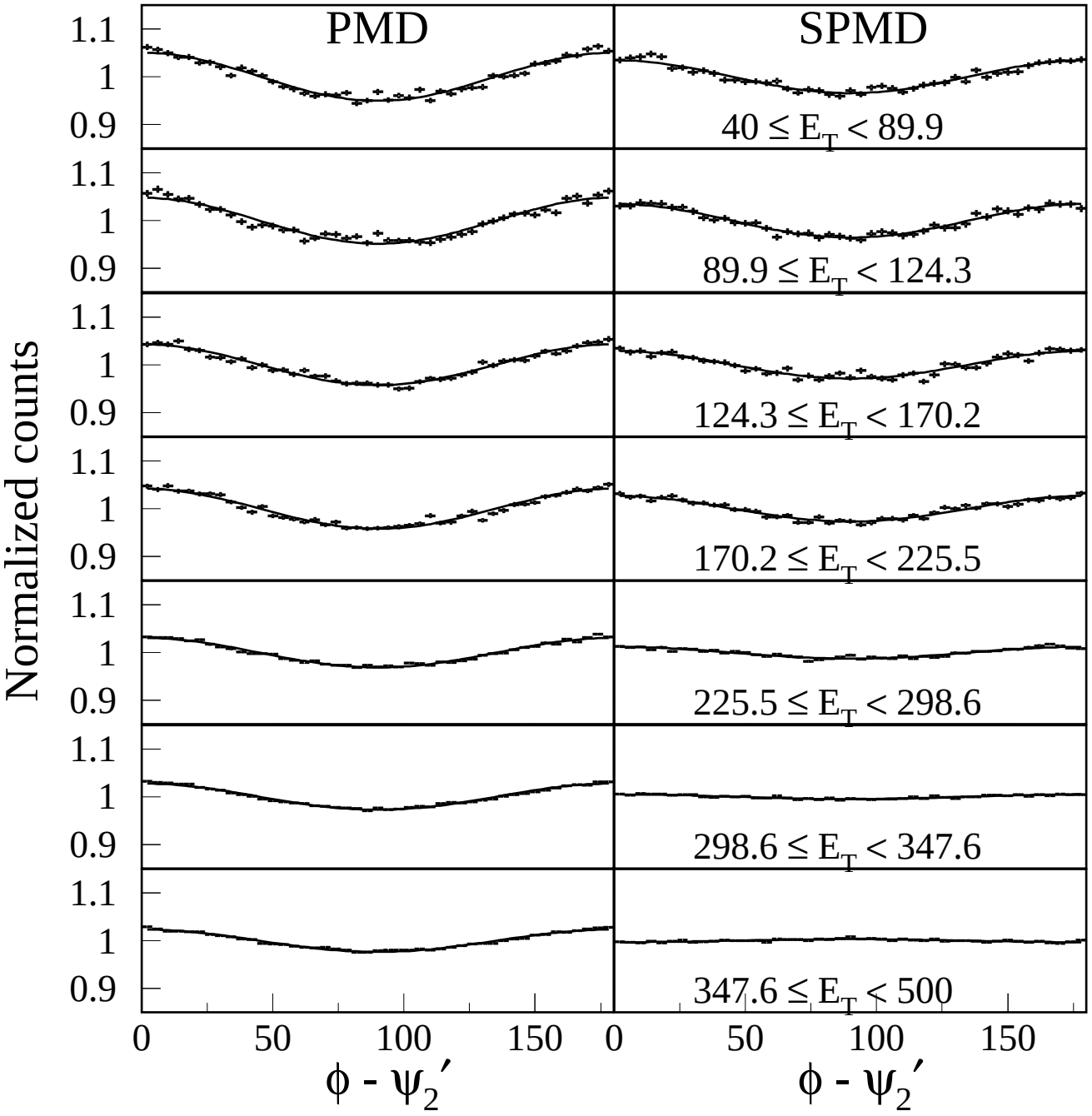

Fig. 4. Distributions of azimuthal angles with respect to the second order event plane, ψ_2', (a) for photons in the PMD and (b) for charged particle hits in the SPMD. Results are shown for each centrality selection in the pseudorapidity region $3.25 \leq \eta \leq 3.75$. The fit results using Eq. 4 are also shown.

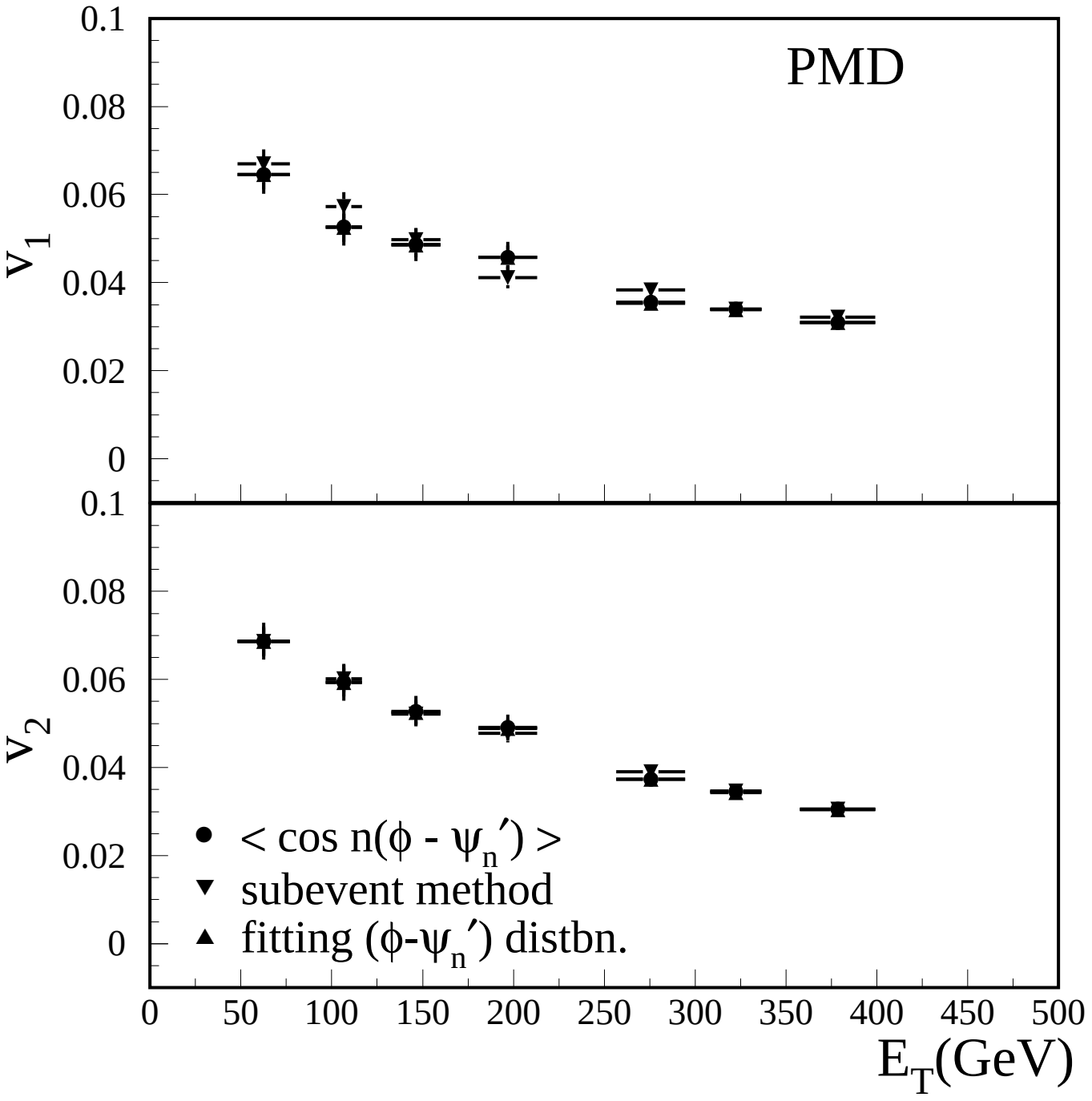

Fig. 5. Comparison of the v_n of the photon azimuthal distributions obtained by different methods for different centralities. The v_n have been determined by (i) calculating the average Fourier term (circles), (ii)the subevent method (inverted triangles), (iii) fitting the $\phi - \psi'_n$ distributions (triangles). The errors are statistical

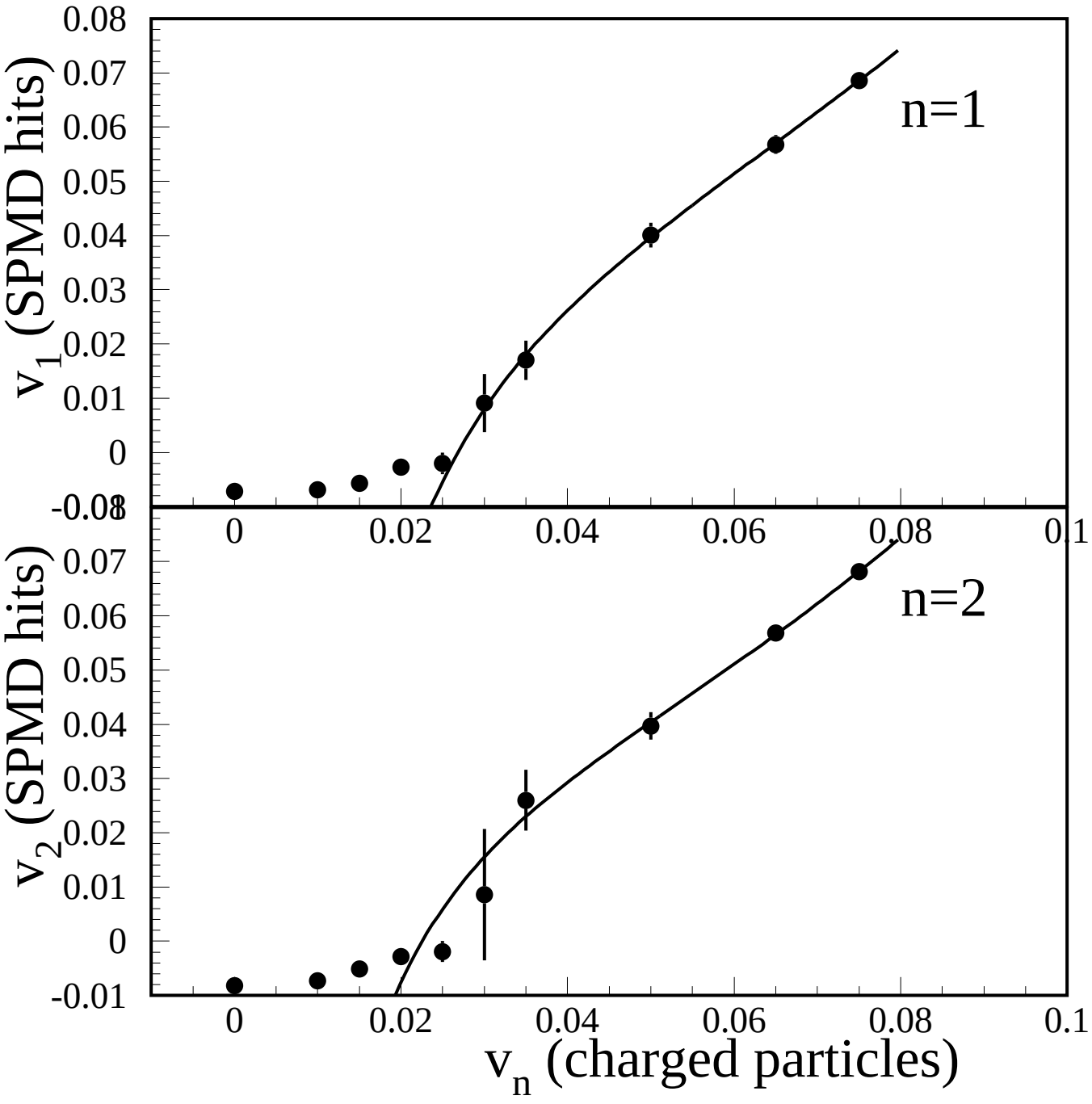

Fig. 6. The anisotropy coefficients extracted from the SPMD hits is shown for different values of initial anisotropy in the charged particles, as obtained in simulations, both for first order and for second order. The solid lines are polynomial fits.

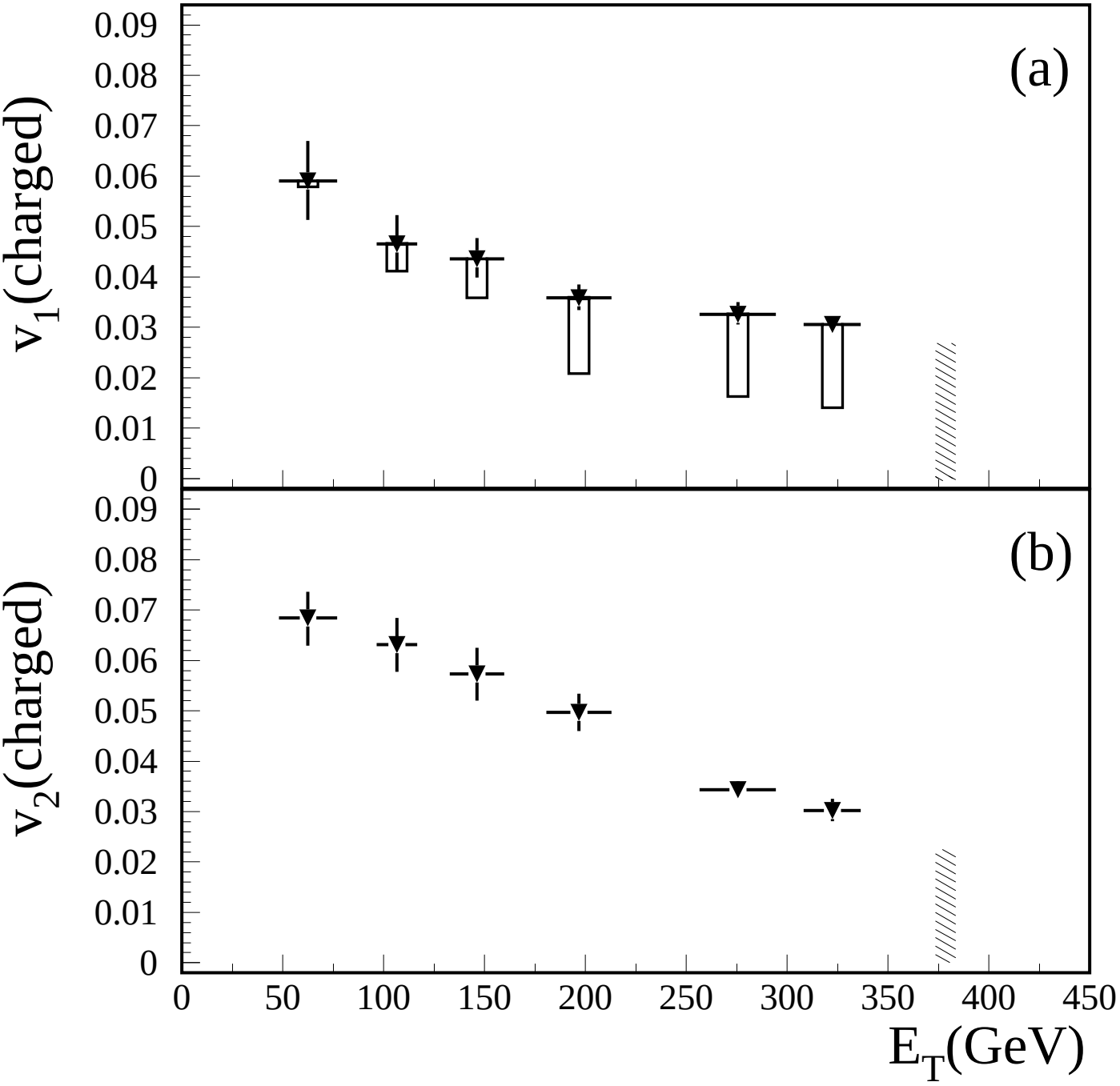

Fig. 7. Anisotropy coefficients of the azimuthal distributions of charged particles in the pseudorapidity region $3.25 \leq \eta \leq 3.75$ for different centralities characterised by the measured transverse energy. (a) First order, v_1, where the open boxes indicate the extent of the total systematic error due to spread in the vertex position. (b) second order, v_2. The shaded region for the most central bin for both orders defines the limit of the anisotropy values consistent with a measured value equal to zero.

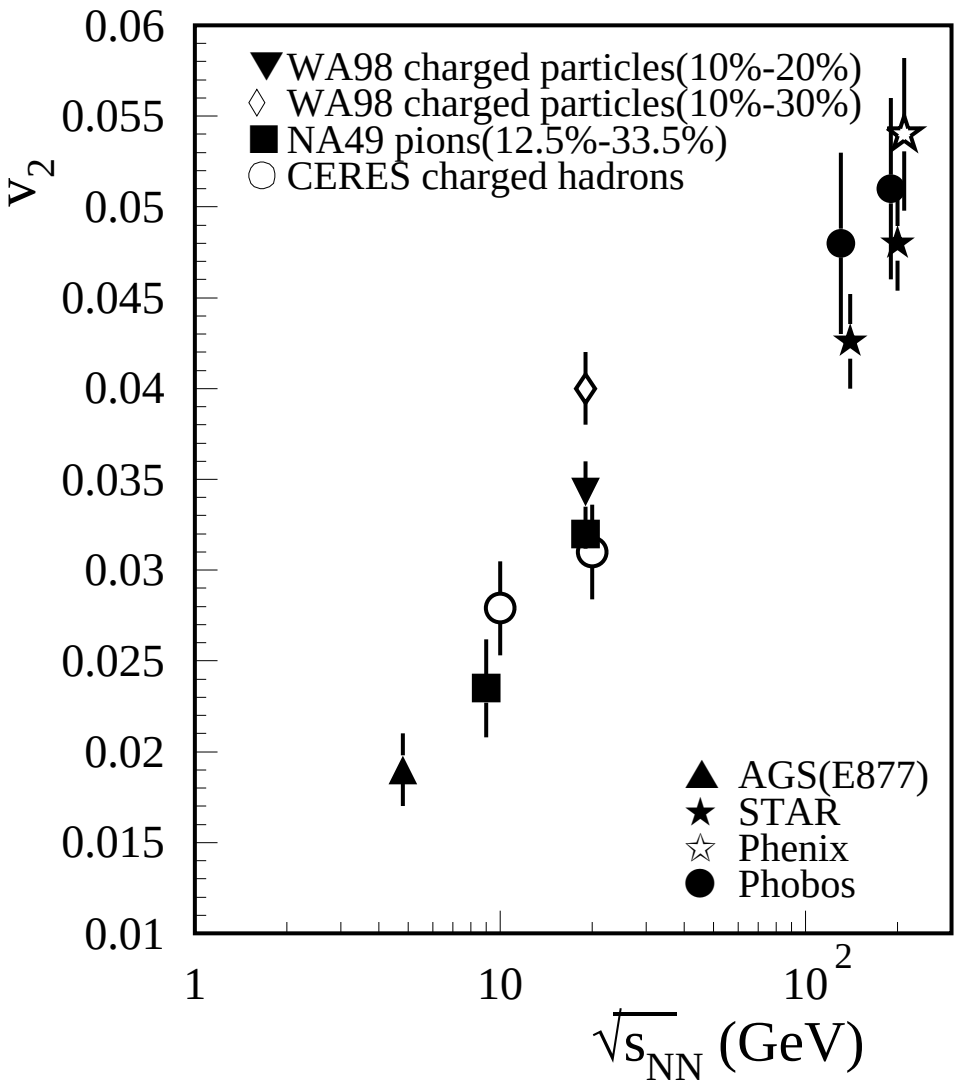

Fig. 8. Second order coefficient for different centre of mass energies. The results of the present work are for charged particles and are shown for two different centrality classes.

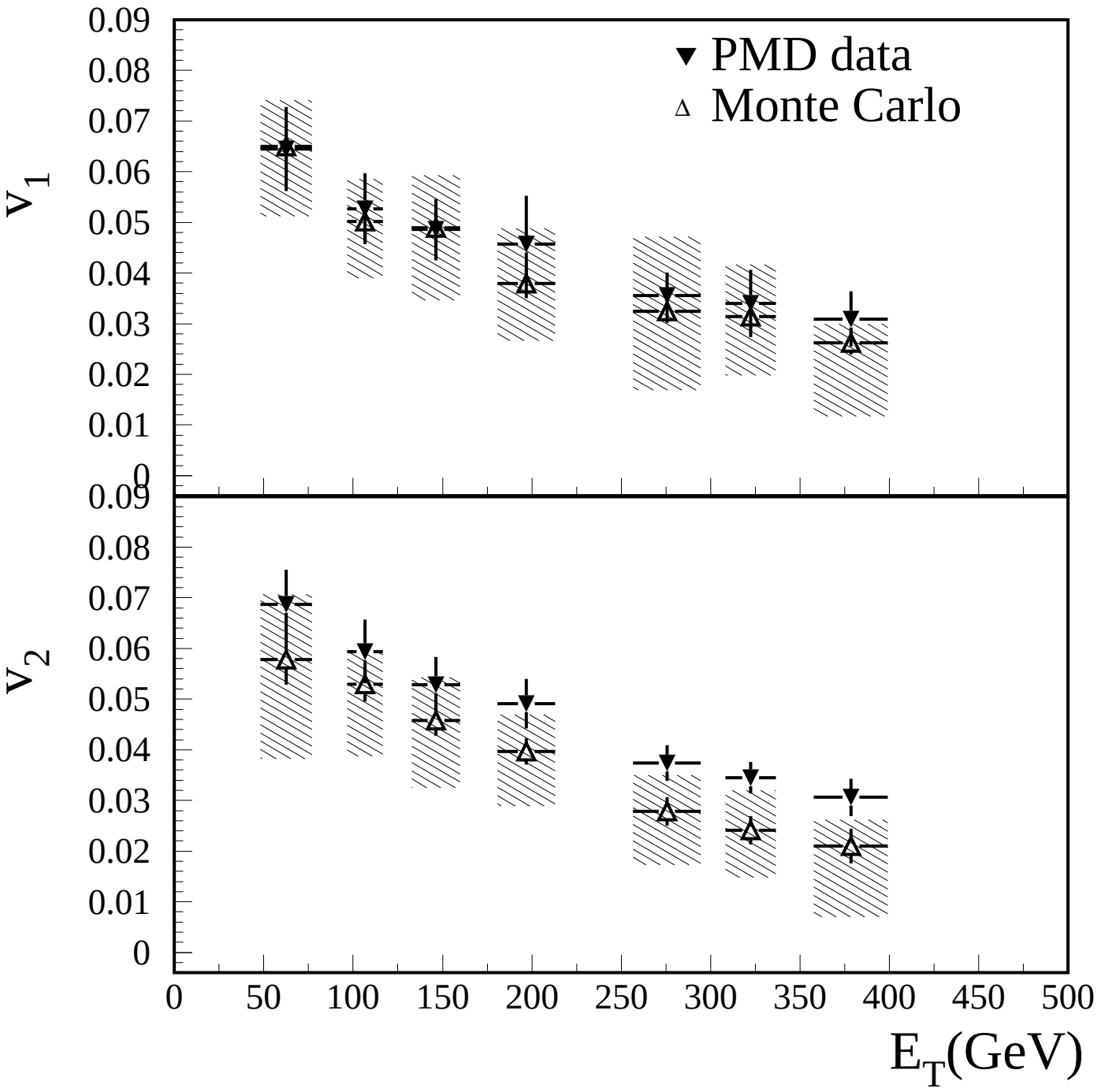

Fig. 9. (a) First order, v_1, and (b) second order, v_2, anisotropy coefficients of the azimuthal distributions of photons in the pseudorapidity region $3.25 \leq \eta \leq 3.75$ for different centralities are shown by filled triangles. Statistical and systematic errors are added in quadrature and shown as bars on the filled triangles. Open triangles are the most probable values of v_n(PMD) as expected from the simulation. The shaded regions indicate the simulation uncertainties given in detail in Tables 2 and 3.

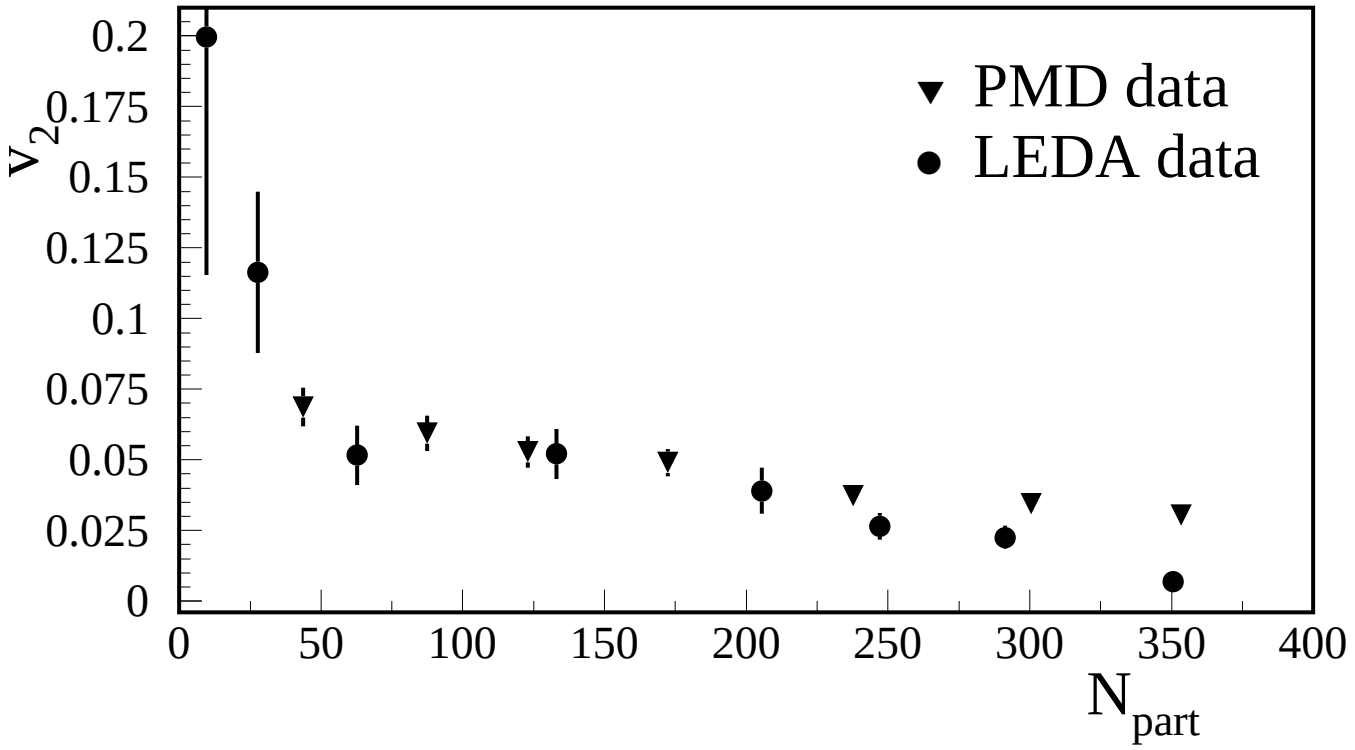

Fig. 10. Anisotropy coefficients of the azimuthal distributions of photons in the PMD are shown by filled triangles. The coefficients for photons (measured in LEDA) are obtained using the reaction plane from the plastic ball and are also shown for comparison. The errors shown are quadratic sum of statistical and systematic errors.